metals

MDPI

Article

The Role of Parent Phase Topology in Double Young–Kurdjumow–Sachs Variant Selection during Phase Transformation in Low-Carbon Steels

Leo A. I. Kestens [1,2,*], Tuan Nguyen-Minh [1] and Roumen H. Petrov [1,2]

[1] Metal Science and Technology, Department of Electromechanical, Systems and Metal Engineering, Ghent University, Technologiepark 46, B-9052 Ghent, Belgium; tuan.nguyenminh@ugent.be (T.N.-M.); roumen.petrov@ugent.be (R.H.P.)
[2] Department of Materials Science and Engineering, Delft University of Technology, Mekelweg 2, 2628 CD Delft, The Netherlands
* Correspondence: leo.kestens@ugent.be

Abstract: The present paper investigates the role of parent phase topology on a crystallographic variant selection rule. This rule assumes that product phase nuclei appear at certain grain boundaries in the parent structure, such that a specific crystallographic orientation relationship is observed with both parent grains at either side of the grain boundary. The specific crystallographic orientation correspondence considered here is the Young–Kurdjumow–Sachs (YKS) orientation relationship <112>90° (which exhibits 24 symmetrical equivalents). The aforementioned relationship is characteristic of phase transformations in low-carbon steel grades. It is shown that, for different parent phase textures, ~20% of the grain boundaries comply with the double YKS condition allowing for a tolerance of 5°, ignoring the presence of topology in the parent phase microstructure. The presented model allows for connecting the presence of a specific parent phase topology with the condition of the double YKS variant selection rule in a number of practical cases: (i) for hot rolled Ti–Interstitial Free (IF) steel with and without Mn addition, (ii) for cold rolled IF steel exhibiting very strong texture memory after forward and reverse $\alpha \rightleftharpoons \gamma$ phase transformation and (iii) for a martensitic transformation in a Fe–8.5% Cr steel. It is shown that the double YKS variant selection criterion may explain several specific features of the observed transformation textures, while assuming a non-correlated arbitrary pair topology of the parent austenite structure (implying that for N parent orientations N/2 pairs are selected in an arbitrary manner).

Keywords: crystallographic texture; low-carbon steel; phase transformation; Young–Kurdjumow–Sachs orientation relations; texture memory

Citation: Kestens, L.A.I.; Nguyen-Minh, T.; Petrov, R.H. The Role of Parent Phase Topology in Double Young–Kurdjumow–Sachs Variant Selection during Phase Transformation in Low-Carbon Steels. *Metals* **2022**, *12*, 939. https://doi.org/10.3390/met12060939

Academic Editor: Frank Czerwinski

Received: 8 April 2022
Accepted: 25 May 2022
Published: 30 May 2022

1. Introduction

The phase transformation in low-carbon steels from the high temperature austenite phase to different potential product phases (ferrite, martensite or bainite) provides one of the most powerful levers to control the mechanical properties of steel through thermo-mechanical processing. This phase transformation also affects the crystallographic texture, as it is well-known that product phase orientations bear a specific orientation relationship with parent austenite crystal orientations [1]. For low-carbon steels, the YKS orientation relationship (<211>90°) [2,3] is often considered the prevailing orientation correspondence between parent and product crystal orientations. It can be noticed that depending on the cooling rate, the product microstructures may vary widely, from polygonal ferrite under a slow cooling condition to lath type martensite after quenching. The product textures, however, are far less dependent on the cooling rate and the texture of hot rolled steel sheets is often characterized by a {112}<110> component if the parent austenite texture exhibits the typical β-fiber FCC rolling texture, in first approximation irrespective of the

cooling rate. Although the reason for this is not fully understood, it is probably related to the fact that specific orientation relationships allow for a (semi-)coherent crystallographic interface between parent and product crystals, which may drastically reduce the activation energy [4].

Because of crystal symmetry, each parent austenite orientation will produce 24 symmetrically equivalent product orientations following the YKS orientation relationship in the absence of variant selection. Variant selection occurs because of an external boundary condition that breaks the crystal symmetry, e.g., an applied load may favor the nucleation of one variant orientation at the expense of another one because of the local strain energy balance [5]. One of the more peculiar instances of variant selection is observed in cold rolled ultra-low-carbon or Interstitial Free (IF) steels that are recrystallization annealed in the full austenite domain. As the structure undergoes a forward and reverse $\alpha \rightleftharpoons \gamma$ transformation, in the absence of variant selection, each initial crystal orientation would be subdivided into 24^2 final orientations. This would not only give rise to significant grain refinement in the final microstructure, but also to a final texture that is all but random, even when the initial texture at the onset of the double phase transformation exhibits the typical <111>//ND fiber recrystallization texture of an IF steel [1]. Experimental evidence, though, shows nearly the opposite behavior: after the forward and reverse $\alpha \rightleftharpoons \gamma$ phase transformation the final texture very much resembles the <111>//ND recrystallization texture that appeared at the onset of phase transformation, or is even stronger in some cases. This phenomenon is called texture memory and it is a typical example of variant selection [6–11]. It was shown by Hutchinson and Kestens [12] that texture memory can be explained by the nucleation of ferrite grains at parent austenite grain boundaries, which allows for a double YKS orientation relationship during cooling [13]. It implies that nucleation is highly favored at special parent grain boundaries such that in the set of 24 × 24 potential product orientations at both sides of the boundary, there is at least one common product orientation for two adjacent parent crystals. A double YKS orientation relationship was experimentally supported by direct observation of early ferrite nuclei appearing at parent austenite grain boundaries in a Fe–Co alloy [14]. In the case of a double YKS orientation relationship, the breaking of the perfect cubic symmetry between the variants is the consequence of the nucleation at grain boundaries.

The occurrence of a double YKS orientation relationship was already modeled by Tomida [8–10] and it was shown that better correspondence with experimental results could be obtained by combining the double YKS variant selection rule with the elastic accommodation of transformation stresses at grain boundaries in case of a displacive transformation. However, the model of Tomida does not include the consideration of a specific topology of the parent structure. It is the aim of the present work to model the effect of double YKS variant selection (neglecting other sources of variant selection) by statistically representing a texture as a set of N crystal orientations. It intends to investigate the effect of topological aspects of the parent microstructure by considering a specific subset of pairs of parent grains from the set of all possible $N(N-1)/2$ pairs.

2. Results

2.1. Fraction of Double YKS Orientation Relations

The requirement to preserve a fully coherent interface of a new nucleus appearing at a grain boundary of the parent structure can only be fulfilled (i) for a subset of special austenite grain boundaries and (ii) for a subset of specific product orientations that exhibit a YKS orientation relationship at either side of the boundary.

Figure 1 shows the fraction of parent austenite grain boundaries that fulfill the special condition to allow for a double YKS orientation relationship as a function of the allowed tolerance within the YKS correspondence. These data were obtained by considering all possible non-identical misorientation pairs in a set of N discrete orientations (i.e., $(N/2)(N-1)$ orientation pairs) distributed over triclinic Euler Space ($0 \leq \varphi_1 \leq 2\pi$; $0 \leq \Phi$, $\varphi_2 \leq \pi/2$), with N = 1000. For the random texture, the discrete orientations were uniformly distributed

over Euler Space, whereas the β-fiber and the Cube fiber textures were obtained by discretizing a Gaussian ODF of width 10° in N = 1000 discrete orientations. For all parent orientation pairs, the 24 × 2 product variants were calculated, producing 24^2 misorientations. If at least one of these misorientations was smaller than the set tolerance, then the parent pair was considered to comply with the double YKS condition.

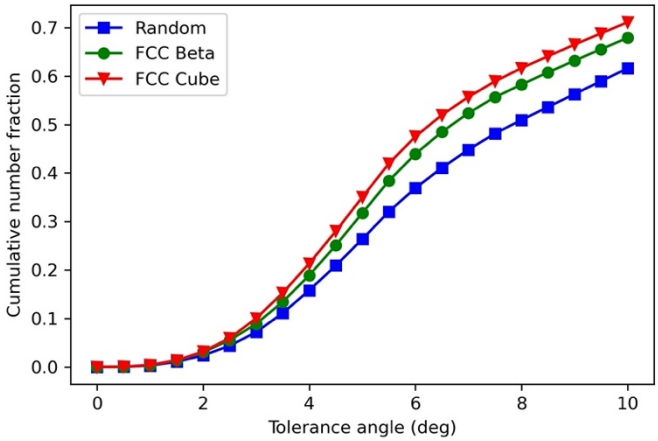

Figure 1. Number fraction of parent austenite GBs allowing for a double YKS orientation relationship as a function of the allowed tolerance.

It can be observed that, for a random parent austenite texture, approximately 60% of the austenite GBs allow for a double YKS orientation relationship observing a tolerance of 10°, which corresponds to the report of Tomida et al. [11]. The data in Figure 1 show that the largest fraction of double YKS GBs can be observed for the single component Cube texture, which can be understood by the fact that for a single component texture, with increasing misorientation tolerance, an increasing fraction of parent misorientation pairs will be considered low angle misoriented pairs for which all possible product variants are common variants. The FCC cube and β-fiber textures were considered because it is well-known that these are the typical austenite textures before the onset of phase transformation in hot rolled low-carbon steel sheets after the final rolling pass.

2.2. Transformation Textures of the IF Hot Rolled Steel Sheet

Yoshinaga et al. [15,16] published a very extensive study on the role of thermo-mechanical processing during hot rolling on texture development in Ti–IF steels with and without Mn addition. In Figure 2 the hot rolling textures from a Ti–IF steel (Figure 2a) and a Mn-added Ti–IF steel (Figure 2b) are compared. Figure 2a shows the typical transformation texture obtained after hot rolling in the austenite domain with the finishing pass below the Tnr temperature (Tnr = the temperature below which interpass recrystallization is no longer complete). This steel exhibits a weak maximum (3 mrd) in the vicinity of the {114}<110> component and the typical morphology of a transformed FCC β fiber texture, corresponding to the fact that the hot rolling was partially carried out below the Tnr temperature. The texture that was observed in the Mn-added IF steel, cf. Figure 2b, exhibits a strong maximum (10 mrd) in the {112}<110> component and virtually no intensity on the γ fiber (<111>//ND).

Figure 3a shows the presumed β fiber austenite parent texture prior to phase transformation. This texture was obtained by applying a simulation of plane strain compression with true strain = 2 with the full constraint Taylor model (FCT) and with octahedral slip systems {111}<110> on 3744 random orientations. The rolling texture exhibits maxima at the Cu {112}<111>, the S {123}<634> and the Bs {110}<112> components. If this texture is rotated around the 24 symmetrical equivalents of the <112>90° axis angle pair, which corresponds to the YKS orientation relationship without variant selection, the texture in Figure 3b is obtained. This is a much weaker texture than the parent texture in Figure 3a,

as each parent orientation gave rise to 24 product orientations according to the 24-fold symmetry of the cubic lattice. If, however, the double YKS model is applied to the parent texture in Figure 3a, the product texture in Figure 3c is produced. This texture was obtained by dividing the parent β fiber texture of the deformed austenite, represented by 3744 discrete orientations in 1872 pairs of two randomly selected orientations. Among these pairs, the ones that allow for a double YKS orientation relationship were identified, and for these pairs the product orientations were calculated that are common between the two parent grains.

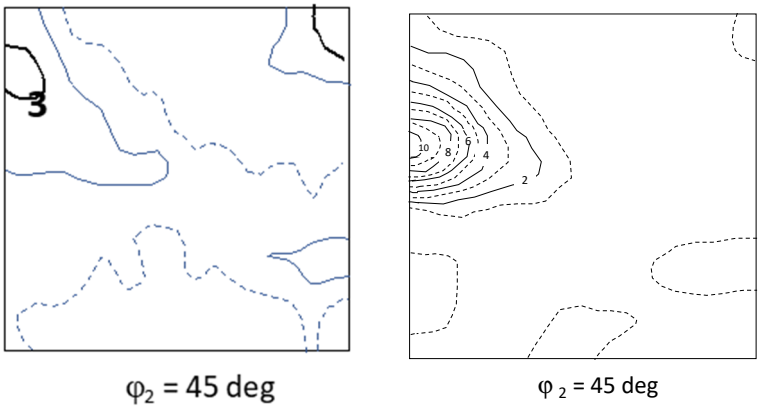

Figure 2. $\varphi_2 = 45°$ sections of (**a**) Ti–IF steel and (**b**) Mn-alloyed Ti–IF steel after austenitic hot rolling, partially below the Tnr temperature. ODFs extracted from [15].

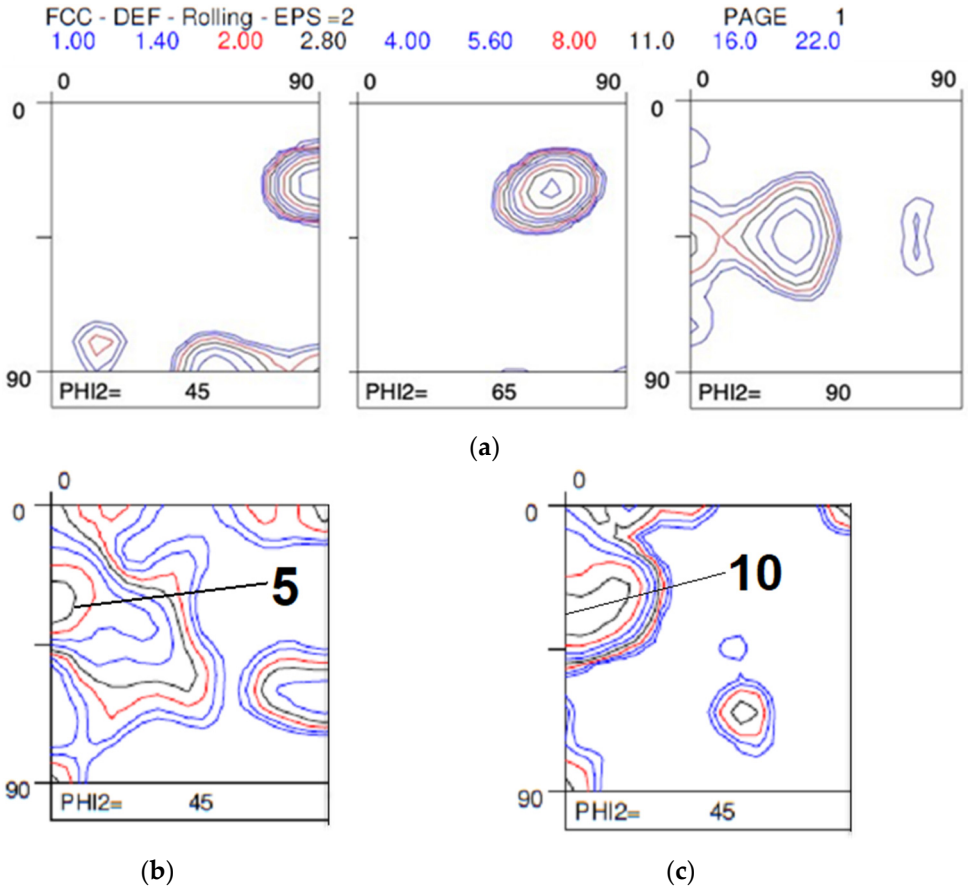

Figure 3. (**a**) Simulated FCC β fiber texture after a rolling reduction at true strain = 2; (**b**) the modeled BCC product texture without variant selection and (**c**) with double YKS variant selection.

2.3. Texture Memory during Forward and Reverse $\alpha \rightleftharpoons \gamma$ Transformation

Figure 4a shows a typical γ fiber texture (<111>//ND) of an IF steel after recrystallization annealing in the ferrite domain. It can be reasonably assumed that this is the starting texture at the onset of a forward and reverse $\alpha \rightleftharpoons \gamma$ phase transformation such as the one studied by Yoshinaga et al. [17]. If it is additionally assumed that the forward $\alpha \rightharpoonup \gamma$ transformation occurs without variant selection, then the texture in Figure 4b is obtained. The hypothesis of absence of variant selection during the forward transformation is based on the consideration that this transformation occurs during heating, and hence the role of activation energy, and the corresponding importance of a coherent interface of transformation nuclei, is probably less important than for a transformation occurring during cooling. The ODF in Figure 4b logically exhibits a <110>//ND fiber because of the $\{111\}_\gamma//\{110\}_\alpha$ parallelism of the YKS orientation relationship. The texture in Figure 4b was derived by discretizing the initial texture from Figure 4a in 2000 individual orientations and applying the <211>90° YKS orientation operators on these orientations, resulting in a set of 24 × 2000 = 48,000 produced austenite orientations. It is important to emphasize that in this list of 48,000 orientations the grains appear in groups of 24 crystal orientations that have one single ferrite crystal as common parent. Hence, in the sequence of austenite orientation, the subset $g_i{}^\gamma$, $g_{i+1}{}^\gamma$, … $g_{i+24}{}^\gamma$, with (i − 1) mod 24 = 0, has a common ferrite parent crystal orientation.

When the double YKS model is applied for the reverse $\alpha \leftharpoondown \gamma$ transformation, the mathematically identical texture is obtained as the one shown in Figure 4a, which demonstrates that in this case we obtain ideal texture memory. This was obtained by pairing the grains of the 48,000 parent austenite orientations and calculating the common product orientations for these pairs that comply with the double YKS condition. Unlike the simulation in Figure 3c, in this case the pairs were not selected randomly, but the ordering sequence of the list of austenite parent grains was preserved, thus mimicking the microstructural proximity of high temperature austenite grains originating from one single low temperature ferrite.

However, when the set of 48,000 orientations of the high temperature austenite texture was randomly scrambled (hereby destroying the topology of the microstructure obtained after forward $\alpha \rightharpoonup \gamma$ transformation) and then the double YKS variant selection was applied to this set of 48,000 randomly sequenced austenite parent grains, this resulted in the ferrite texture in Figure 4c after reverse $\alpha \leftharpoondown \gamma$ transformation.

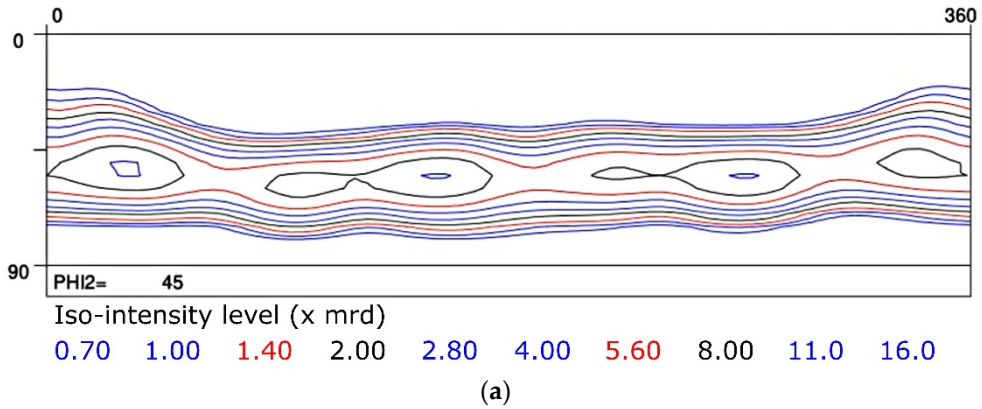

(**a**)

Figure 4. *Cont.*

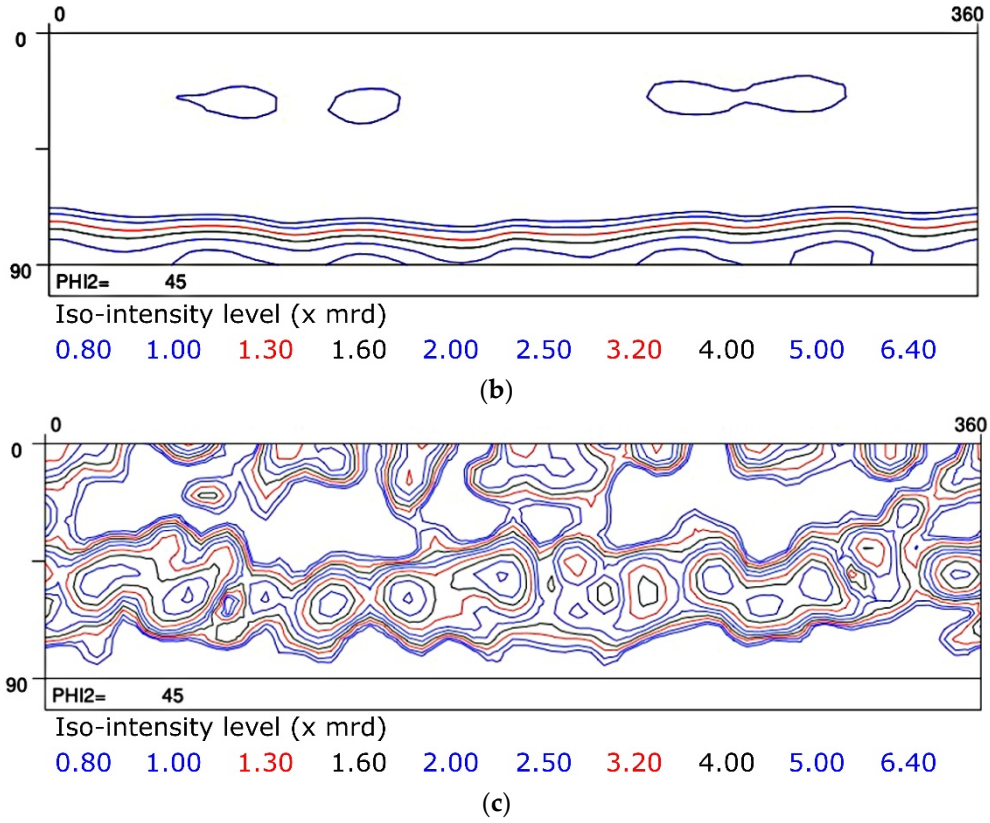

Figure 4. (**a**) Typical {111} deep drawing texture of an IF steel grade; (**b**) FCC texture derived from (**a**) by applying the YKS orientation operator without variant selection; (**c**) BCC texture derived by applying the double YKS variant selection rule to a sample of discrete orientations representative of the texture shown in (**b**) after random scrambling of the sequence of these orientations.

2.4. Martensitic High Strength Steel

Figure 5a shows the orientation contrast map of a martensitic high strength Fe–8.5%Cr alloy. The orientation map was acquired with the EDAX-TSL-Data Collection software v7.3 (EDAX/TSL Inc., Draper, UT, USA) attached to a Quanta 450 FEG–SEM (ThermoFisher Scientific, Eindhoven, Netherlands) operating at 20 kV with a probe current of 2.4 nA. The sample was prepared according to the standard steel sample preparation routes with a final polishing step with colloidal silica (OPS) for 25 min and a force of 15 N, cleaned in an ultrasound bath, flushed with pure ethanol and dried with hot air. The parent austenite structure was reconstructed with OIMv8.6® software (EDAX/TSL Inc., Draper, UT, USA) based on the YKS orientation relationship, cf. Figure 5b. The OIM maps contained ~1.4×10^6 pixels and were recorded with a step size of 0.4 µm. Figure 6a exhibits the texture of the martensite product phase. This texture was calculated by imposing a Gaussian ODF with a spread of 5° on each of the ~1.4×10^6 pixels of the OIM in Figure 5a. When the same procedure was applied to the reconstructed parent phase scan in Figure 5b the texture in Figure 6b was obtained, which exhibits the typical β fiber texture of a rolled metal sheet with an FCC crystal structure. Subsequently, the ODF of the reconstructed parent phase was discretized in a sample set of 2000 orientations, each with the same weight factor. When the YKS orientation operator was applied to these 2000 orientations without variant selection, a new set of 48,000 (=24 × 2000) orientations was produced that gave rise to the ODF in Figure 6c. When the YKS operator was applied to the same set but with the double YKS variant selection rule, according to the same procedure as described in Section 2.2, the ODF in Figure 6d was obtained. It needs to be emphasized that all calculations were carried out in the triclinic Euler space ($0° < \varphi_1 < 360°$, $0° < \Phi$, $\varphi_2 < 90°$) without considering sample symmetry. However, for the final result of simulated and measured textures, orthorhombic sample symmetry was applied in order to improve data statistics, and thus the ODFs in

Figure 6 are represented in the [0°, 90°] restricted zone of Euler space. For calculation of the continuous ODFs of the textures in Figure 6a, a Gaussian spread of 5° was assumed.

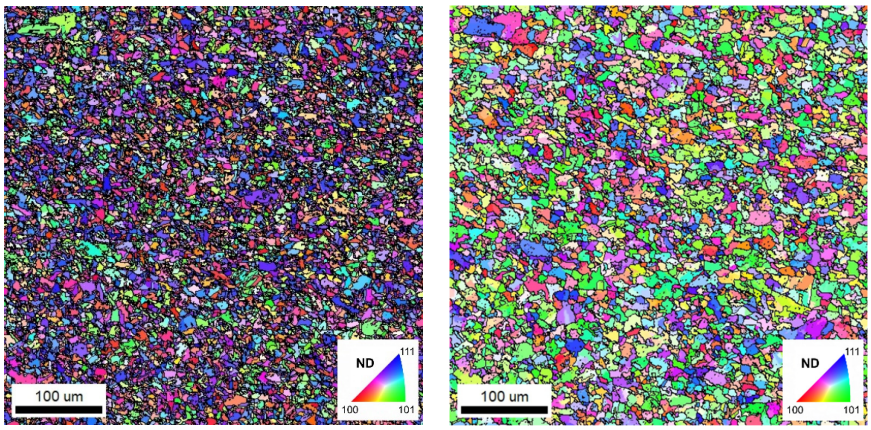

(**a**) (**b**)

Figure 5. (**a**) Experimentally measured OIM map of a martensitic Fe-8.5Cr alloy and (**b**) reconstructed parent austenite map obtained with OIMv8.6® software.

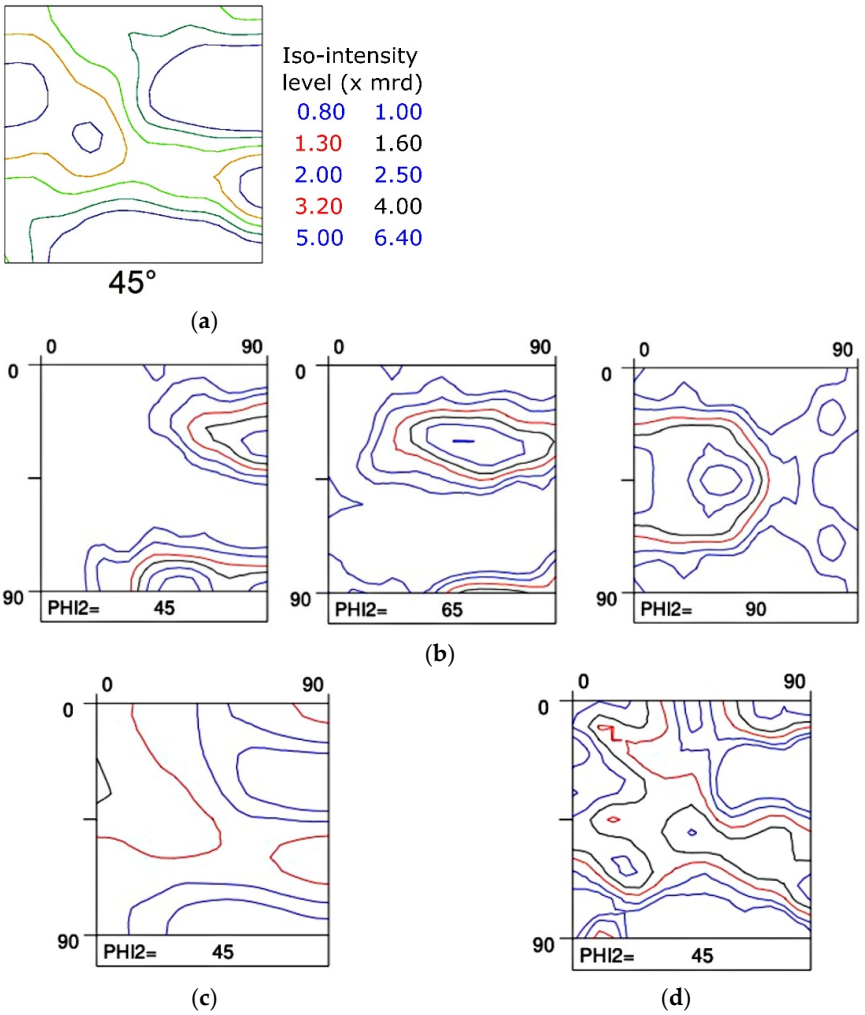

Figure 6. (**a**) Measured product martensite texture corresponding to Figure 5a; (**b**) Reconstructed austenite texture corresponding to the map in Figure 5b; Simulated product texture (**c**) without variant selection and (**d**) applying the double YKS variant selection rule. Level lines: 0.8–1.0–1.3–1.6–2.0–2.5–3.2–4.0–5.0–6.4.

3. Discussion

It can obviously be observed that the model without variant selection (Figure 3b) best resembled the product texture of the Ti–IF steel (Figure 2a) whereas the model with double YKS variant selection (Figure 3c) more resembles the product texture of the Mn-added IF steel (Figure 3b). It should be mentioned that the Ti–IF steel in Figure 2a was hot rolled with the last pass at 913 °C, after which it was subjected to a coiling simulation at 700 °C. This produced an equiaxed polygonal ferrite hot band structure with an average grain size of 23 μm [15]. Conversely, the Mn-added Ti–IF steel in Figure 2b was finish rolled at 865 °C followed by a coiling simulation at 450 °C, which gave rise to a bainitic hot band structure [15]. It was already observed by Hutchinson and Kestens [12] that displacive transformations enhance the conditions for texture memory in IF steel, which they associate with the double YKS variant selection mechanism. The reason is that a displacive transformation occurs at a lower temperature and thus with a lower activation energy. Hence, the double YKS orientation relationship, ensuring a (semi-)coherent interface to a larger degree than the single YKS orientation, would be of more critical importance for the displacive than for the diffusive transformation. Therefore, the double YKS type variant selection was more pronounced in the Mn-added IF steel.

Perfect texture memory is observed if the topology after the forward $\alpha \rightharpoonup \gamma$ transformation is preserved in the high temperature austenite phase, i.e., if the austenite grains nucleating from one single parent ferrite grain remain clustered at high temperatures. However, a different texture arises if the topology of the high temperature austenite phase is not preserved and the austenite grains are randomly scrambled after forward transformation. In this case, it can be observed that the modeled texture in Figure 4c after forward $\alpha \rightharpoonup \gamma$ (without variant selection) and reverse $\alpha \leftharpoondown \gamma$ transformation (with double YKS variant selection) exhibits texture memory only to a certain degree. The final texture in Figure 4c still reproduces the initial γ fiber texture prior to transformation, albeit with a reduced intensity of 5 mrd (compare figure Figure 4a with Figure 4c). Surprisingly, a θ fiber texture (<001>//ND) is also observed in the final product texture with a maximum of ~3.2 mrd at the rotated cube component. The result presented here demonstrates the influence of local topology on the double YKS variant selection. For example, it can be imagined that the local topology of the austenite phase is (partially) destroyed by grain growth at elevated temperatures. It is shown here that such a phenomenon would mitigate the appearance of texture memory. As it is impossible to assess the true topology of the high-temperature austenite structure, only two limiting cases were considered here: one with perfect preservation and one with complete removal of the local topology.

Alternatively, it needs to be mentioned that Yoshinaga observed an increased incidence of the θ fiber components after $\alpha \rightleftharpoons \gamma$ phase transformation in IF steel [1,17]. This was particularly true for the surface texture [15,18]. It was argued by Yoshinaga that either the crystallographic dependence of the surface energy and/or the release of normal transformation stresses at the surface might be responsible for the selection of {001} crystal orientations in the vicinity of the surface. Gautam et al. [19,20] convincingly reported that surface energy dependence can indeed enhance the selection of {001} oriented surface crystal orientations. The fact, however, that the double YKS variant selection mechanism might also contribute to enhancing θ fiber {001} components was not previously considered.

When comparing the modeled product textures (Figure 6c,d) derived from the reconstructed parent ODF in Figure 6b, it is not immediately obvious which of the modeled textures (without variant selection, Figure 6c, or with double YKS variant selection, Figure 6d) best corresponds to the measured product texture in Figure 6a. In terms of intensity, the double YKS modeled ODF in Figure 6d best corresponds to the experimental counterpart. Moreover, the experimental texture exhibits a local maximum in the {332}<113> component, which is absent in the ODF that was modeled without variant selection (Figure 6c), but which is approximately present in the ODF modeled with double YKS variant selection (Figure 6d).

For higher alloyed steels, it is often claimed that the preferred orientation correspondence is the Nishiyama–Wasserman orientation (NW) relationship ($\{111\}_\gamma//\{110\}_\alpha$ $<112>_\gamma//<111>_\alpha$) rather than the YKS correspondence ($\{111\}_\gamma//\{110\}_\alpha$ $<110>_\gamma//<111>_\alpha$) [2,3]. If the parent texture is reconstructed on the basis of the NW relationship, then the texture in Figure 7a is obtained. This ODF, similarly to the texture in Figure 6b, exhibits a β fiber, but in addition features a maximum of 4 mrd at the cube component. When this NW reconstructed austenite texture is employed as the parent texture to which the double NW operator is applied, then the texture in Figure 7b is derived, which exhibits an even more pronounced maximum at the {332}<113> component. However, it also features a maximum at the rotated cube component, which is not observed in the experimental product texture in Figure 6a. It is well-known that the rotated cube component of the product texture is strongly enhanced by the presence of a cube component in the parent texture. Apparently the cube component of the parent texture is overestimated by the reconstruction algorithm in OIMvs.8.6®.

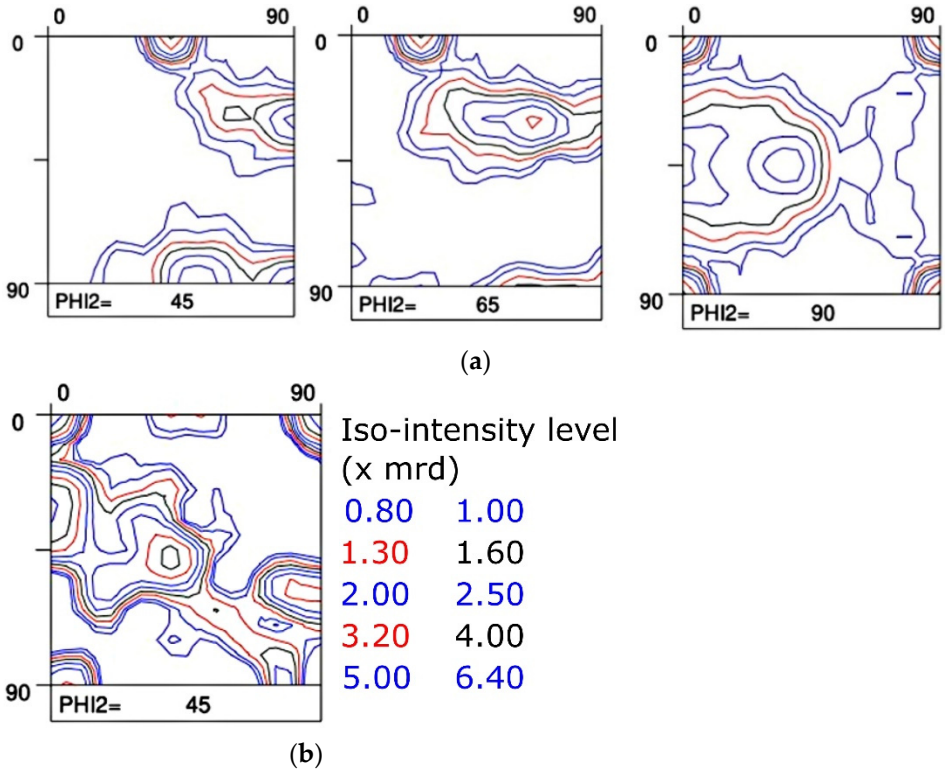

Figure 7. (**a**) Reconstructed austenite texture corresponding to the map in Figure 5b applying the NW orientation relationship (φ_2 = 45°, 65° and 90° sections) and (**b**) φ_2 = 45° product texture derived from (**a**) by applying the double NW variant selection rule.

In applying the double YKS orientation relationship, there is an implicit topological hypothesis assuming that the product orientations nucleate at the parent structure grain boundaries. In the examples considered here, the double YKS condition was applied to a set of N parent orientations. It was deliberately chosen not to consider all possible $(N^2 - N)/2$ pairs of two dissimilar orientations in order to avoid statistically diluting the variant selection to the point that the result would be indistinguishable from the no-variant selection case. Moreover, pairing each crystal to any other crystal in the set would not represent the relevant topology of a real microstructure. As an alternative, the set of N orientations was scrambled in a random sequence and N/2 pairs were considered, to which the double YKS condition was applied (with the exception of the texture memory case in Section 2.2, where groups of 24 austenite variants produced during the forward $\alpha \rightharpoonup \gamma$ transformation were kept together, reflecting the particular topology of the case). It needs to be assessed whether or not the proposed manner of considering the parent structure topology is appropriate for the present purpose of texture modeling.

4. Conclusions

A simple model was presented to assess the consequences of variant selection based on a specific mechanism that applies to special austenite grain boundaries that allow for a YKS orientation relationship for a product nucleus at both sides of the boundary, i.e., the so-called double YKS orientation relationship. The model presents a mean-field approach whereby the basic building blocks consist of the individual crystallographic orientations that represent a specific texture. The model was applied to three specific examples: (i) the hot band texture of Ti–IF steel with and without Mn, (ii) forward and reverse $\alpha \rightleftharpoons \gamma$ phase transformation in an IF steel and (iii) the austenite to martensite transformation in a Fe–8.5%Cr alloy. In all these cases the double YKS variant selection mechanism was able to explain some particular features of the transformation texture, including the dominance of the {112}<110> component in the hot band texture of the Mn-alloyed Ti–IF steel, the strong texture memory effect after the forward and reverse $\alpha \rightleftharpoons \gamma$ phase transformation in cold rolled IF steel and the presence of the {332}<113> component in the martensite transformation texture of a Fe–8.5%Cr alloy. The model also revealed the importance of the topology of the parent microstructure. Better simulation could be obtained not by considering all possible orientation pairs of a set of N parent orientations, but by sampling a subset of $N/2$ pairs among all possible pairs.

Author Contributions: L.A.I.K. was responsible for conceptualization, carrying out the model calculations and drafting the manuscript hereby supported by T.N.-M. T.N.-M. was responsible for gathering the experimental data presented in Section 2.3 and R.H.P. was responsible for gathering and processing the experimental data presented in Section 2.4. All authors have read and agreed to the published version of the manuscript.

Funding: This research received no external funding.

Institutional Review Board Statement: Not applicable.

Informed Consent Statement: Not applicable.

Data Availability Statement: Not applicable.

Acknowledgments: Felipe Castro Cerda and Eliseo Hernández Durán are gratefully acknowledged for numerous inspiring discussions on the topic of phase transformations. The authors are indebted to Olga Kachko for assisting with the Fe–8.5%Cr alloy.

Conflicts of Interest: The authors declare no conflict of interest.

References

1. Yoshinaga, N.; Ushioda, K.; Itami, A.; Akisue, O. $\alpha + \gamma$ and γ Phases Annealing in Ultra Low-carbon Sheet Steels. *ISIJ Int.* **1994**, *34*, 33–42. [CrossRef]
2. Young, J. The Crystal Structure of Meteoric Iron as Determined by X-Ray Analysis. *Proc. R. Soc. Lond.* **1926**, *112*, 630–641. [CrossRef]
3. Kurdjumow, G.; Sachs, G. Über den Mechanismus der Stahlhärtung. *Z. Physik* **1930**, *64*, 325–343. [CrossRef]
4. Offerman, S.E.; Van Dijk, N.H.; Sietsma, J.; Grigull, S.; Lauridsen, E.M.; Margulies, L.; Poulsen, H.F.; Rekveldt, M.T.; Van der Zwaag, S. Grain nucleation and growth during phase transformations. *Science* **2002**, *298*, 1003–1005. [CrossRef] [PubMed]
5. Nguyen-Minh, T.; Sidor, J.J.; Petrov, R.H.; Kestens, L.A.I. Occurrence of shear bands in rotated Goss ($\{1\,1\,0\}\langle 1\,1\,0\rangle$) orientations of metals with bcc crystal structure. *Scr. Mater.* **2012**, *67*, 935–938. [CrossRef]
6. Tomida, T.; Wakita, M.; Yoshida, M.; Imai, N. A variant selection rule in transformation in steel and prediction of transformation texture. *Mater. Sci. Forum* **2010**, *638–642*, 2846–2851. [CrossRef]
7. Lischewski, I.; Gottstein, G. Nucleation and variant selection during the α-γ-α phase transformation in microalloyed steel. *Acta Mater.* **2011**, *59*, 1530–1541. [CrossRef]
8. Tomida, T.; Wakita, M.; Yasuyama, M.; Sugaya, S.; Tomota, Y.; Vogel, S.C. Memory effects of transformation textures in steel and its prediction by the double Kurdjumov-Sachs relation. *Acta Mater.* **2013**, *61*, 2828–2839. [CrossRef]
9. Tomida, T. Variant selection mechanism by elastic anisotropy and double K-S relation for transformation texture in steel; difference between martensite and ferrite. *Acta Mater.* **2018**, *146*, 25–41. [CrossRef]

10. Tomida, T.; Vakhitova, E.; Sornin, D.; Wright, J.; François, M.; Onuki, Y.; Hirano, T.; Hoshikawa, A.; Ishigaki, T.; Sato, S. Texture Memory in Si-Mn and ODS Steels Observed In Situ by Pulsed Neutron and Synchrotron X-Ray Diffractions and Prediction by Double Kurdjumov-Sachs Relation: A Concept for Intense Variant Selection. *Metall. Mater. Trans. A* **2021**, *52*, 1368–1381. [CrossRef]
11. Tomida, T.; Vogel, S.; Onuki, Y.; Sato, S. Texture memory in hexagonal metals and its mechanism. *Metals* **2021**, *11*, 1653. [CrossRef]
12. Hutchinson, B.; Kestens, L.A.I. Origins of texture memory in steels. In *Ceramic Transactions, Proceedings of the 15th International Conference on Textures of Materials, ICOTOM 15, Pittsburgh, Pennsylvania, 1–6 June 2008*; Wiley: Hoboken, NJ, USA, 2010; Volume 201, pp. 281–290. [CrossRef]
13. Tomida, T.; Wakita, M.; Yoshida, M.; Imai, N. Quantitative prediction of transformation texture in hot-rolled steel sheets by multiple KS relation. In *Ceramic Transactions, Proceedings of the 15th International Conference on Textures of Materials, ICOTOM 15, Pittsburgh, Pennsylvania, 1–6 June 2008*; Wiley: Hoboken, NJ, USA, 2010; Volume 200, pp. 325–332. [CrossRef]
14. Landheer, H.; Offerman, S.E.; Petrov, R.H.; Kestens, L.A.I. The role of crystal misorientations during solid-state nucleation of ferrite in austenite. *Acta Mater.* **2009**, *57*, 1486–1496. [CrossRef]
15. Yoshinaga, N. Recrystallization and $\alpha \rightarrow \gamma \rightarrow \alpha$ Transformation Textures in Ultra Low Carbon Sheet Steels. PhD Thesis, Ghent University, Ghent, Belgium, 1999.
16. Yoshinaga, N.; Kestens, L.; Vanderschueren, D.; De Blauwe, K.; De Cooman, B. Influence of hot-rolling texture and cold-rolling reduction on planar anisotropy of r-values after recrystallization of IF steels. In Proceedings of the 4th International Conference on Recrystallization and Related Phenomena, Tsukuba City, Japan, 13–16 July 1999; Volume 13, p. 393.
17. Yoshinaga, N.; Inoue, H.; Kawasaki, K.; Kestens, L.; De Cooman, B.C. Factors affecting texture memory appearing through $\alpha \rightarrow \gamma \rightarrow \alpha$ transformation in IF steels. *Mater. Trans.* **2007**, *48*, 2036–2042. [CrossRef]
18. Yoshinaga, N.; Kestens, L.; De Cooman, B.C. $\alpha \rightarrow \gamma \rightarrow \alpha$ transformation texture formation at cold-rolled ultra low carbon steel surfaces. In *Materials Science Forum, Proceedings of the 14th International Conference on Textures of Materials, ICOTOM 14, online 15 September 2005*; Trans Tech Publications Ltd.: Bäch, Switzerland, 2005; Volume 495–497, pp. 1267–1272. [CrossRef]
19. Gautam, J.; Petrov, R.; Kestens, L. Surface texture evolution during α-γ-α transformation in Mn and Al alloyed ultra-low carbon steel. *Mater. Sci. Forum* **2007**, *550*, 503–508. [CrossRef]
20. Gautam, J.; Petrov, R.; Kestens, L.; Leunis, E. Surface energy controlled α-γ-α transformation texture and microstructure character study in ULC steels alloyed with Mn and Al. *J. Mater. Sci.* **2008**, *43*, 3969–3975. [CrossRef]